Comparative study of critical current densities and flux pinning among a flux-grown $NdBa_2Cu_3O_y$ single crystal, melt-textured Nd-Ba-Cu-O, and Y-Ba-Cu-O bulks

T. Higuchi and S. I. Yoo
Railway Technical Research Institute, 2-8-38 Hikari-cho, Kokubunji-shi, Tokyo 185-8540, Japan
and Superconductivity Research Laboratory, International Superconductivity Technology Center, 1-16-25 Shibaura, Minato-ku, Tokyo 105-0023, Japan

M. Murakami
Superconductivity Research Laboratory, International Superconductivity Technology Center, 1-16-25 Shibaura, Minato-ku, Tokyo 105-0023, Japan

(Received 11 May 1998; revised manuscript received 4 September 1998)

We have studied the field and temperature dependence of the critical current density $J_c(B,T)$ for a flux-grown $NdBa_2Cu_3O_y$ single crystal (Nd123SC), melt-textured Nd-Ba-Cu-O (OCMG-Nd-Ba-Cu-O), and Y-Ba-Cu-O (MPMG-Y-Ba-Cu-O) bulks. In the J_c-T curves, an exponential-like behavior in a low-temperature region could be explained in terms of the collective flux creep model, while J_c-T curves in a high-temperature region could well be fitted to the Kim-Anderson creep model. For the scaling of J_c-B curves, power-law relation of $J_c \propto B^{\gamma-1}$ is observed for all the samples in a low-field region in that the exponent γ is roughly $\frac{1}{2}$ for OCMG-Nd-Ba-Cu-O and MPMG-Y-Ba-Cu-O, and 1 for Nd123SC, corresponding to surface pinning and point pinning, respectively. The surface pinning is ascribed to the presence of second-phase particles. In an intermediate field region, the γ values become almost 2 for Nd123SC and OCMG-Nd-Ba-Cu-O, showing that $\Delta\kappa$-point pinning is dominant, which presumably originates from the Nd-Ba substituted regions with depressed T_c. On the basis of our $J_c(B,T)$ analyses, we could classify the B-T phase diagram into several regimes of different dominant pinning mechanisms. [S0163-1829(99)04502-6]

I. INTRODUCTION

High-pinning performance of LRE-Ba-Cu-O (LRE is light rare-earth elements of La, Nd, Sm, Eu, Gd) superconductors,[1–4] which were melt processed in a reduced-oxygen atmosphere, is closely related to the presence of secondary peak effect in the J_c-B curves. The peak effect is also observed in the $NdBa_2Cu_3O_y$ (Nd123) single crystals grown by a traveling-solvent floating-zone method[5] and a self-flux method.[6] Unlike the Y-Ba-Cu-O, which forms only a stoichiometric $YBa_2Cu_3O_y$ (Y123) compound, the LRE-Ba-Cu-O systems exhibit a $LRE_{1+x}Ba_{2-x}Cu_3O_y$ type solid solution.[7] Egi *et al.*[5] and Wu Ting *et al.*[8] found that Nd123 single crystals contain small clusters 10–50 nm in diameter, which have Nd content slightly higher than that of the Nd123 matrix and thus exhibit lower T_c. Such localized Nd-rich clusters are superconducting in low fields and will be driven normal with increasing field, thereby act as field-induced pinning centers. Thus, the presence of Nd-rich clusters has been proposed to be the source of the secondary peak effect in the Nd-Ba-Cu-O. Later, this idea was verified by Chikumoto *et al.*[9] with high-temperature annealing experiments in that the peak effect disappeared when compositional fluctuation in the matrix was annihilated by high-temperature annealing.

The secondary peak effect has also been observed in Y123 single crystals,[10–12] melt-textured Y-Ba-Cu-O bulks with relatively small amounts of the Y_2BaCuO_5 (Y211) second phase[13] and irradiated Y123 single crystals.[14] The peak effect is also termed ''fishtail'' and is often observed in various superconducting materials, although its origin is still controversial. In general, the source of the peak effect is twofold differentiated by its temperature dependence. When the peak field is temperature independent, it is ascribed to the matching effect between the flux-line lattice (FLL) spacing and the average defect spacing. For Bi-Sr-Ca-Cu-O, temperature independent peak effect has successfully been explained in terms of dimensional crossover from three-dimensional (3D) to 2D of FLL.[15] In most cases for Y123 related materials, however, the peak field is temperature dependent, for which several pinning mechanisms have been proposed, e.g., vortex-phase crossover and field-induced pinning based on granular superconductivity.

Krusin-Elbaum *et al.*[10] interpreted the fishtail effect as a change in magnetization relaxation due to the crossover from single vortex to collective pinning. In Ref. 10, a mirror image, in which a larger current density leads to a smaller creep rate, was presented as an experimental evidence for 3D collective pinning, and the fishtail peak was ascribed to a change in the vortex-vortex interaction from a small to large bundle.

Daeumling, Seuntjens, and Larbalestier[11] explained the fishtail effect in terms of granular superconductivity. With increasing magnetic field, superconductivity in the oxygen deficient region with depressed T_c is strongly suppressed, which leads to an increase of the elementary pinning force, and, therefore, the critical current density increases with field. Wen *et al.*[13] have shown that the fishtail effect cannot be explained by the vortex-phase crossover referring their experimental results, in which the fishtail effect is greatly enhanced by extra oxygen deficiencies. Klein *et al.*,[12] on the basis of the fact that the magnetization curves measured at different elapsed times could be scaled onto a single master curve, also concluded that the fishtail effect is related to the

TABLE I. Processing conditions and sample dimensions for Nd123SC, OCMG-Nd-Ba-Cu-O, and MPMG-Y-Ba-Cu-O.

Sample	Atmosphere	Dimensions (mm)	T_c (K)
Nd123SC	0.1%O_2-Ar gas	0.80×0.80×0.30	93.2
OCMG-Nd-Ba-Cu-O	1%O_2-Ar gas	0.92×1.54×0.51	93.9
MPMG-Y-Ba-Cu-O	Air	1.08×1.13×1.12	91.6

property of an elementary pinning center. They suggested that the fishtail effect is due to the flux pinning caused by a spatial fluctuation of the Ginzburg-Landau parameter (or appreciated as $\Delta\kappa$ pinning) in a low-field region and percolation in a high-field region. Recently, Erb *et al.*[16] found that the fishtail peak was not observed in a pure Y123 single crystal when it was grown in a $BaZrO_3$ crucible and fully oxygenated. They also showed that the fishtail peak appeared when the sample was slightly deoxygenated. These results obviously support the fact that the fishtail effect is not intrinsic to the Y123 materials or the vortex phase but originates from the defects or weak superconducting regions, which can be sorted into two groups: local oxygen-deficient regions and weak-superconducting regions caused by chemical contamination either from raw materials or crucibles. As mentioned previously, for the case of LRE-Ba-Cu-O materials, however, local weak-superconducting regions are the LRE rich clusters caused by LRE-Ba substitution, which is supported by the fact that extra deoxygenation did not enhance but rather smeared the peak effect.[1] For some LRE-Ba-Cu-O samples, it should be noted that oxygen-deficient regions or chemically contaminated regions are also present depending on the processing conditions, which will complicate J_c-B properties such that a plateaulike broad peak or even multiple peaks are observed in some crystals.[17] It is also important to note that the optimum oxygen-annealing conditions are dependent on the x value of $LRE_{1+x}Ba_{2-x}Cu_3O_y$ solid solution. Thus, the function of LRE-rich clusters as pinning centers is dependent on the oxygenation levels for both the matrix and the clusters, which should be born in mind when we try to understand the pinning mechanism of LRE-Ba-Cu-O superconductors.

In the melt-processed LRE-Ba-Cu-O the second-phase particles of $LRE_4Ba_2Cu_2O_{10}$ (LRE422) for La, Nd, or LRE_2BaCuO_5 (LRE211) for Sm, Eu, and Gd are also found to act as effective pinning centers particularly in a low-field region,[18] which is analogous to the function of Y211 second-phase particles in the Y123 bulk materials melt grown with several methods like melt textured growth (MTG),[19] quench and melt growth (QMG),[20] and melt powder melt growth (MPMG).[21] These materials frequently exhibit a shoulder or a plateau in the J_c-B curves in a high-temperature region and even a fishtail peak when the amount of Y211 second phase trapped in the Y123 is small. Therefore, in addition to Y211, local oxygen-deficient or other defect (impurity) regions in Y123 can act as pinning centers, showing that the kind of dominant pinning centers can vary depending on the microstructure, temperature, and field strength. Hence, it is important to compare $J_c(B,T)$ characteristics among various systems with well-characterized microstructures, which may allow us to identify dominant pinning mechanism in the B-T phase diagram, and will also be informative for further development of high performance LRE-Ba-Cu-O superconducting materials.

In the present study, $J_c(B,T)$ characteristics were studied for a Nd123 single crystal, melt-processed Nd-Ba-Cu-O, and melt-processed Y-Ba-Cu-O bulk materials with different microstructural features. In order to clarify the effect of flux creep on the $J_c(B,T)$ properties, we also measured the time decay of the magnetization $M(t)$ for a wide temperature and field range.

For analyzing $J_c(T)$ curves, we employed several theories including the Kim-Anderson model,[22] vortex glass,[23] and collective-pinning.[24–26] Similarly, for the $J_c(B)$ and $F_p(B)$ curves, scaling parameters were determined by fitting the data to the appropriate scaling relationship. With such data analyses, we compared the flux-pinning characteristics for the present samples. Finally, we could successfully classify the B-T phase diagram into several regimes based on the dominant pinning mechanism.

II. EXPERIMENT

$NdBa_2Cu_3O_y$ single crystal (Nd123SC) was flux grown in a yttria-stabilized zirconia (YSZ) crucible using the flux composition of Nd:Ba:Cu=1:15:34 in flowing 0.1%O_2-Ar. The details of the crystal-growth conditions are described elsewhere.[27] As-grown crystals were oxygenated in flowing pure O_2 by slowly cooling from 500 to 250 °C for 100 h.

We have also prepared Nd-Ba-Cu-O and Y-Ba-Cu-O with the melt-textured process. Bulk Nd-Ba-Cu-O sample was grown by the oxygen-controlled melt-growth (OCMG) method[1] with the nominal composition of Nd:Ba:Cu =1.8:2.4:3.4, which corresponds to the molar ratio of $NdBa_2Cu_3O_y$:1/2$Nd_4Ba_2Cu_2O_{10}$=100:40. The melt-growth process was performed in a 1%O_2-Ar atmosphere. The grown samples were oxygenated at 300 °C for 100 h. Bulk Y-Ba-Cu-O sample was melt processed by the MPMG method[21] with the nominal composition of Y:Ba:Cu =1.8:2.4:3.4. The samples were melt grown in air and subjected to oxygenation at 400 °C for 100 h.

Sample dimensions and the onset T_c for these three samples are listed in Table I. In the present study, full oxygenation for each sample was aimed. Based on the previous studies on the relation between annealing temperature and oxygen content for $NdBa_2Cu_3O_{7-d}$[28] and $YBa_2Cu_3O_{7-d}$,[29] we employed the temperatures of 300 and 400 °C for OCMG-Nd-Ba-Cu-O and MPMG-Y-Ba-Cu-O, respectively. In contrast, for Nd123SC, which is more difficult to incorporate oxygen, higher temperatures at initial stage were employed, followed by slow cooling from 500 to 250 °C. Compared with the previous results reported by Takita *et al.*,[30] T_c higher than 93 K for the Nd123SC and OCMG-Nd-Ba-Cu-O

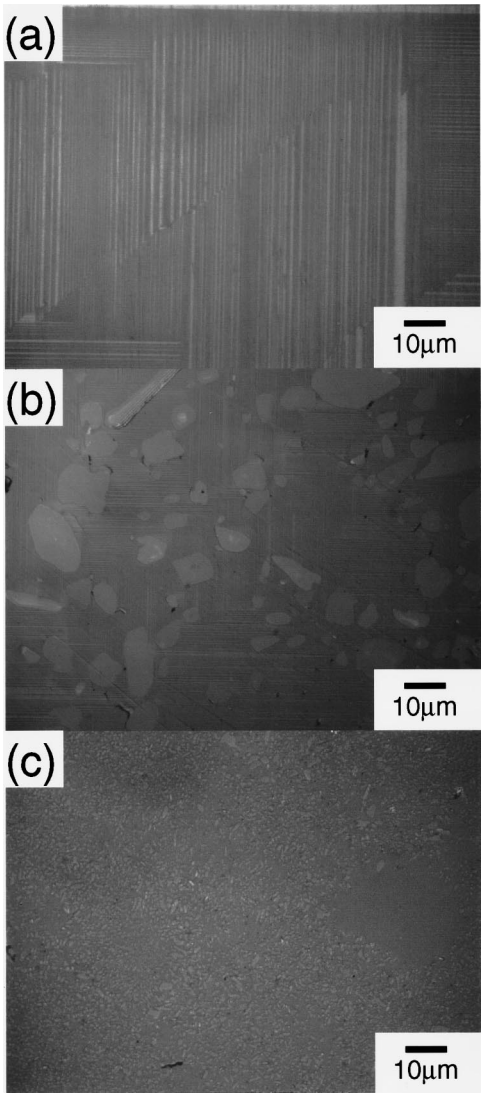

FIG. 1. Optical micrographs under polarized light for (a) Nd123SC, (b) OCMG-Nd-Ba-Cu-O, and (c) MPMG-Y-Ba-Cu-O. Nd123SC exhibits only twin structure. OCMG-Nd-Ba-Cu-O and MPMG-Y-Ba-Cu-O samples contain second-phase particles with respective average diameters of approximately 10 and 1 μm.

indicates that x in the formula $Nd_{1+x}Ba_{2-x}Cu_3O_{7-d}$ is smaller than 0.05.

Figure 1 shows optical micrographs under polarized light for the three samples. Nd123SC exhibits only a twin structure without other appreciable defects, however, scanning tunneling microscopic[8] and transmission-electron microscopic observations[5] confirmed the presence of Nd-rich $Nd_{1+x}Ba_{2-x}Cu_3O_{7-d}$ (Nd123ss) clusters about 10–50 nm in diameter. OCMG-Nd-Ba-Cu-O and MPMG-Y-Ba-Cu-O samples contain second-phase particles with respective average diameters of approximately 10 and 1 μm. In the matrix of OCMG-Nd-Ba-Cu-O, Nd-rich Nd123ss clusters are also present.[9] In MPMG-Y-Ba-Cu-O fine Y211 inclusions are dispersed in the Y123 matrix with fine twin structures. Therefore, microstructural features of three samples are characterized as follows. All the samples contain twin planes. Nd123SC has Nd-rich Nd123ss clusters. OCMG-Nd-Ba-Cu-O has both Nd-rich Nd123ss clusters and large normal-conducting particles. MPMG-Y-Ba-Cu-O contains relatively fine normal conducting particles. Powder x-ray diffraction showed that these second phases were Nd422 for the OCMG-Nd-Ba-Cu-O[18] and Y211 for the MPMG-Y-Ba-Cu-O.[21]

dc magnetization measurements were performed with a quantum design MPMS superconducting quantum interference device (SQUID) magnetometer. Data acquisition was made using a scanning length of 4 cm in a persistent current mode after waiting for 30 s at the target field. Onset T_c data were determined from the magnetization curves measured with a dc field of 10 Oe applied parallel to the c axis ($H \| c$). M-H loops were measured with a maximum applied field of 7 T in a temperature range of 10 to 92 K.

The time decay of magnetization $M(t)$ was measured for 4000 s at various fields ranging from 1 to 5 T and temperatures from 10 to 77 K. In order to ensure full flux penetration, a negative field of -5 T was applied prior to each decay measurement. Onset time of the decay measurements was defined $t_{\rm init}=140$ s by taking account of the time required for field stabilization in the equipment. This value of $t_{\rm init}$ was certified by the fact that the exponent μ values in the relation $M^{-\mu} \propto \ln t$ were almost identical for two different methods, in which μ was determined as to maximize the statistical correlation constant R^2 in the line fitting of $M^{-\mu} \propto \ln t$, or as a slope of $1/S \propto \ln t$ (S: normalized creep rate), as performed by Civale *et al.*[31] J_c values were determined from the M-H loops using the extended Bean model[32] with the following relation:

$$J_c = 20\Delta M/a/(1-a/3b), \tag{1}$$

where J_c is in A/cm^2, ΔM is magnetization hysteresis during increasing and decreasing field processes in emu/cm^3, and a, b ($a \leqslant b$) are cross-sectional sample-dimensions perpendicular to the field and in cm. When an external field H is applied parallel to an infinite superconducting slab, vortices inside the sample is always parallel to the applied field, which allows one to estimate the correct J_c values using the extended Bean model. In practical cases, however, since the sample dimensions are finite, the effect of self magnetic induction (B_s) must be taken into consideration. When H is small, the vortices will be bent owing to B_s.[33,34] In such a case, the contribution of J_c parallel to the c axis (J_c^c) is not negligible compared to that of J_c parallel to the ab plane (J_c^{ab}), and, thus, it is difficult to determine accurate J_c values based on the extended Bean model. For simplicity, hereafter we regard the B_s as an applicability limit for the J_c determination using the extended Bean model, which has previously been employed by Civale *et al.*[14] Since B_s is roughly equivalent to the field that reaches the center of a sample, B_s (in G) is approximated as

$$B_s \approx J_c a/2. \tag{2}$$

At higher fields, the vortices inside the sample tend to align parallel to the external field. In addition, magnetic induction B is almost identical to the external field H due to a relatively small magnetization value M compared with that of B ($=\mu_0 H + M$), for which the extended Bean model is reasonably valid to assess correct J_c values.

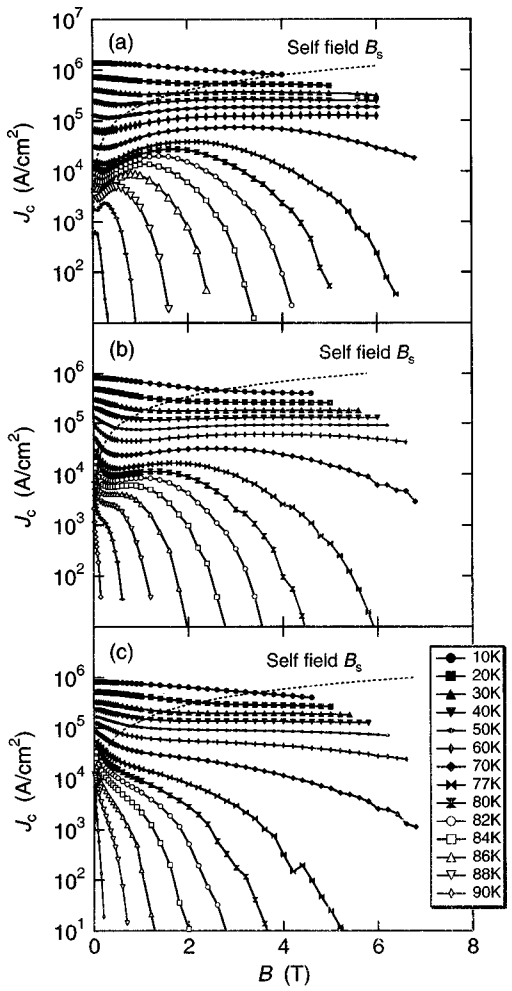

FIG. 2. Semilogarithmic plots of J_c-B curves ($H\|c$) in a temperature range of 10–92 K for (a) Nd123SC, (b) OCMG-Nd-Ba-Cu-O, and (c) MPMG-Y-Ba-Cu-O. The self-field B_s is represented by a dotted line in the figure. Note that the field dependence of J_c is different among these samples. Nd123SC exhibits prominent fishtail peaks in an intermediate-field range at temperatures above 70 K. MPMG-Y-Ba-Cu-O exhibits monotonous decrease in J_c with increasing B in all the temperature range. OCMG-Nd-Ba-Cu-O shows a monotonous decrease in J_c with B at lower fields and a fishtail peak at higher fields when temperature is above 70 K.

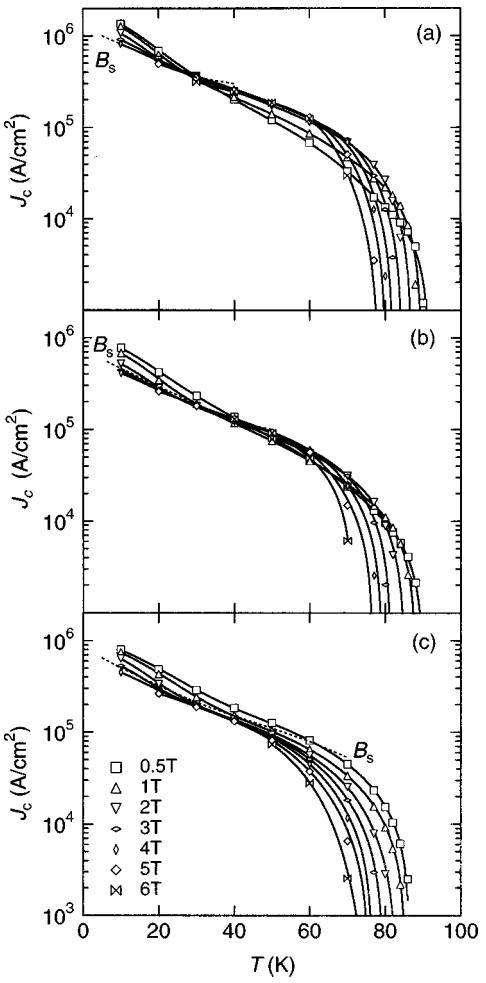

FIG. 3. Semilogarithmic plots of J_c vs T in a field range of 0.5–6 T with $H\|c$ for (a) Nd123SC, (b) OCMG-Nd-Ba-Cu-O, and (c) MPMG-Y-Ba-Cu-O. Here B_s is again represented by a dotted line. For Nd123SC and OCMG-Nd-Ba-Cu-O, the slope of the ln J_c-T plot decreases with increasing B, corresponding to the fishtail peak effect. For MPMG-Y-Ba-Cu-O, however, the slope of the ln J_c-T plot is almost constant.

III. RESULTS AND DISCUSSION

A. $J_c(B,T)$ behaviors

Figure 2 shows semilogarithmic plots of J_c-B curves for three samples. As shown in Fig. 2(a), Nd123SC exhibits prominent fishtail peaks in an intermediate field range at high temperatures above 70 K. In contrast, MPMG-Y-Ba-Cu-O in Fig. 2(c) exhibits a monotonous decrease in J_c with increasing B in all the temperature range, which is quite different from the presence of prominent peaks in Y123 single crystals.[10–12] Both a decrease in J_c with B at lower fields and fishtail peaks at temperatures above 70 K are observed in OCMG-Nd-Ba-Cu-O, as shown in Fig. 2(b), although the peak effect is not so pronounced as to be compared with that of Nd123SC. Here, it is interesting to notice that the J_c-B behavior of OCMG-Nd-Ba-Cu-O shows combined characteristics of Nd123SC and MPMG-Y-Ba-Cu-O.

Figure 3 shows semilogarithmic replots of J_c as a function of temperature for these samples. For all the samples, below 0.5 T J_c decreases monotonously with increasing temperature. The linear relation, which is observed in the plot of ln J_c vs T at temperatures below 70 K, shows an exponential relationship of $J_c \propto \exp(-CT)$, where C is a temperature-independent constant. Further increase in T to the irreversibility temperature $T_{\rm irr}$, however, leads to a considerable depression of J_c. In contrast, above 1 T, each sample shows slightly different J_c-T behavior. For the Nd123SC sample, the slope of the ln J_c-T plot becomes small with increasing B due to the fishtail effect in the J_c-B curves. OCMG-Nd-Ba-Cu-O shows similar J_c-T behavior in that there is a crossover in the J_c-T curves, which is not observed in MPMG-Y-Ba-Cu-O exhibiting a monotonous decrease in J_c with increasing T.

B. Temperature dependence of J_c

A general expression of the volume pinning force $F_p(B,T)$ is given in the form

$$F_p(B,T)=F_{p0}[1-(T/T_c)^2]^m b^\gamma(1-b)^\delta. \quad (3)$$

From the relation $J_c \equiv F_p/B$, one can obtain

$$J_c(B,T)=J_{c0}[1-(T/T_c)^2]^{m'}B^{\gamma-1}(1-b)^\delta, \quad (4)$$

where J_{c0} and F_{p0} are independent of B and T, m, γ, and δ are scaling parameters ($m'=m-\gamma$), and b is a reduced magnetic induction B/B_{c2} (B_{c2}: upper critical field).[35] The temperature dependence of J_c is then given by $J_c(T) \approx J_{c0}[1-(T/T_c)^2]^{m'}$. As discussed in our previous paper,[36] however, a simple linear relationship could not be found on the plot of $\ln J_c$ vs $\ln[1-(T/T_c)^2]$. Although J_c exhibited a monotonous decrease with increasing temperature, each curve was not characterized by a single parameter but consisted of three different regimes depending on temperature: low, intermediate, and high T regimes exhibiting a different temperature dependence.

As shown in Fig. 3, an exponential relation of $J_c(T) \propto \exp(-CT)$ is observed at temperatures below 70 K, while no such relation is established both in low- and high-temperature regions. Feigel'man *et al.*[24] theoretically predicted that an exponential relation in $J_c(T)$ would be observed in a collective pinning regime. Manuel, Aguillon, and Senoussi,[37] concluded that an exponential temperature dependence of J_c is equivalent to a logarithmic dependence of the pinning potential on the defect-vortex distance in the flux-creep model. Dorosinskii *et al.*[38] demonstrated that a wide Gaussianlike distribution of pinning energies causes the exponential decay of J_c with increasing T in Y123 crystals. However, in our case, the treatment based on such exponential J_c-T relation cannot cover the whole temperature range. In a low-field and low-temperature region, underestimate of J_c due to the self-field might cause discrepancy from the exponential relation. It is also true that a simple exponential expression fails to describe an abrupt decrease in J_c at temperatures above 70 K, where thermal-activation energy is large. Hereafter, quantitative analyses are performed to fit the experimental data to various proposed models by considering the flux-creep effect.

1. Kim-Anderson model

In the Kim-Anderson model,[22] on the assumption that an apparent pinning potential U is linearly reduced with increasing the current J, $U(J)$ has the form

$$U(J)=U_0[1-J/J_{c0}], \quad (5)$$

where U_0 and J_{c0} are pinning potential and critical current density in the absence of flux creep, respectively. Combining Eq. (5) with the Arrhenius relation for the vortex hopping leads to the well-known Kim-Anderson flux-creep relation

$$J_c(T)=J_{c0}[1-(T/U_0)\ln(t/t_{\rm eff})], \quad (6)$$

and the normalized creep rate $S(T)$ $[\equiv -(\partial \ln J/\partial \ln t)_{B,T}]$ is given by

$$S(T)=-T/[U_0-T\ln(t/t_{\rm eff})], \quad (7)$$

where $t_{\rm eff}$ is an effective attempt time. Equation (6) shows that J_c is greatly reduced due to the flux creep when U_0 is small and T is large. One can also see that J_c should decrease linearly with T in a low T region, where U_0 is almost temperature independent, leading to a convex curvature in the $\ln J_c$-T plot. However, a concave curvature is observed in the experimental $\ln J_c$-T curves shown in Fig. 3.

2. Collective creep

Thompson *et al.*[39] adopted the following inverse power-law form based on the vortex-glass[23] and the collective-pinning/collective-flux-creep[24–26] theories:

$$U(J)=(U_0/\mu)[(J_{c0}/J)^\mu-1], \quad (8)$$

with the characteristic exponent μ. One advantage of this expression is that it contains almost all the $U(J)$ functions. For example, the Kim-Anderson model is the case for $\mu=-1$. The relation of $U(J)=U_0\ln(J_{c0}/J)$ adopted by Zeldov *et al.*[40] or Maley *et al.*[41] is also obtained for $\mu=0$. Using this $U(J)$ relation, a more general form for $J_c(T)$ is given by

$$J_c(T)=J_{c0}/[1+(\mu T/U_0)\ln(t/t_{\rm eff})]^{1/\mu}, \quad (9)$$

and thus

$$S(T)=-T/[U_0+\mu T\ln(t/t_{\rm eff})]. \quad (10)$$

The exponent μ is an important parameter to characterize both the relaxation and vortex dynamics. Phenomenologically, $\mu=-1$ gives a straight line, while $\mu<-1$ and $\mu>-1$ give respective convex and concave curves in the plot of M vs $\ln t$. In the collective-pinning theory,[24–26] three different pinning regimes of single-vortex pinning, small- and large-flux bundles are characterized by $\mu=1/7$, 3/2, and 7/9, respectively.

Figure 4 shows time decay of normalized magnetization in a temperature range of 10–77 K for these samples at an applied field of 4 T, which is believed to be sufficiently high enough to neglect the self-field effect even at 10 K. Here, the slope of the M-$\ln t$ curve gives the normalized creep rate S according to the equation $S \equiv -(\partial \ln J/\partial \ln t)_{B,T} \approx (dM/d\ln t)/M_{\rm init}$. As a general trend for all the samples, the relaxation behavior can be summarized as follows. At low temperatures, the slope is quite small and almost independent of temperature, although a large increase in the slope is observed at temperatures above 60 K for MPMG-Y-Ba-Cu-O and above 70 K for Nd123SC and OCMG-Nd-Ba-Cu-O.

To enlighten the difference in the relaxation behavior among these samples, we deduced the temperature dependence of the normalized creep rate S and the linear coefficient μ in the relation $M^{-\mu} \propto \ln(t)$. A least-square method was used to obtain a μ value according to the method by Civale *et al.*[31] and Thompson *et al.*[42] in which the μ value was determined by varying hypothetical values to minimize the quantity $(1-R^2)$, where R^2 is a statistical correlation constant and ideally unity for a perfect fitting. Next, S is obtained from the slope of $\ln M$ vs $\ln t$ plot using the least-square method. Thus, obtained temperature dependence of μ and S is displayed in Fig. 5. For all the samples, it should be noted that μ ranges from 0 to 3 in a low-temperature range, while μ is negative in a high-temperature region. S-T curves for all the samples show almost temperature-independent values, ranging from 0.02 to 0.04 roughly up to 60 K for Nd samples and to 50 K for Y samples. These results are con-

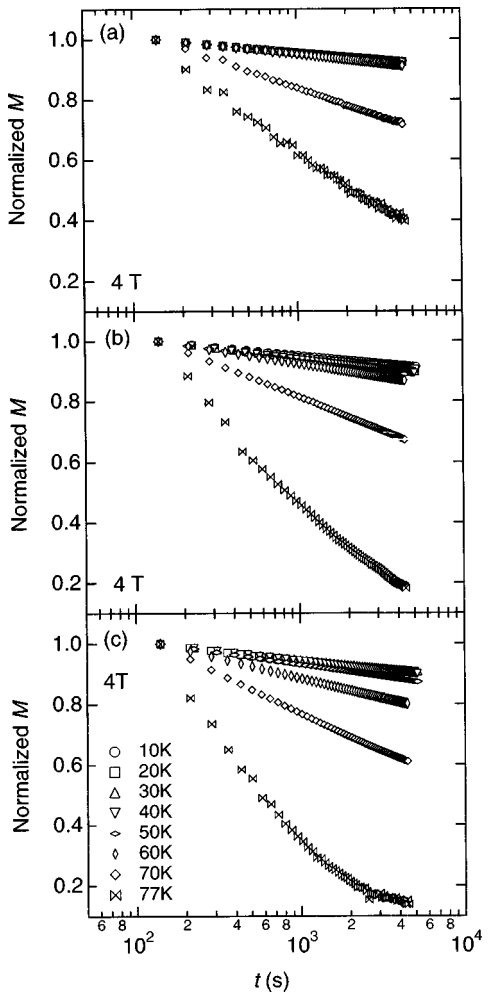

FIG. 4. Time decay of M at temperatures from 10 to 77 K for (a) Nd123SC, (b) OCMG-Nd-Ba-Cu-O, and (c) MPMG-Y-Ba-Cu-O. The data at 4 T were employed, since it is higher than the self-field even at a temperature as low as 10 K. The M value is normalized by the initial M value for all the temperatures. At temperatures below 50 K, the slope is small and almost independent of temperature. In contrast, a considerable increase in the slope is observed at temperatures above 60 K.

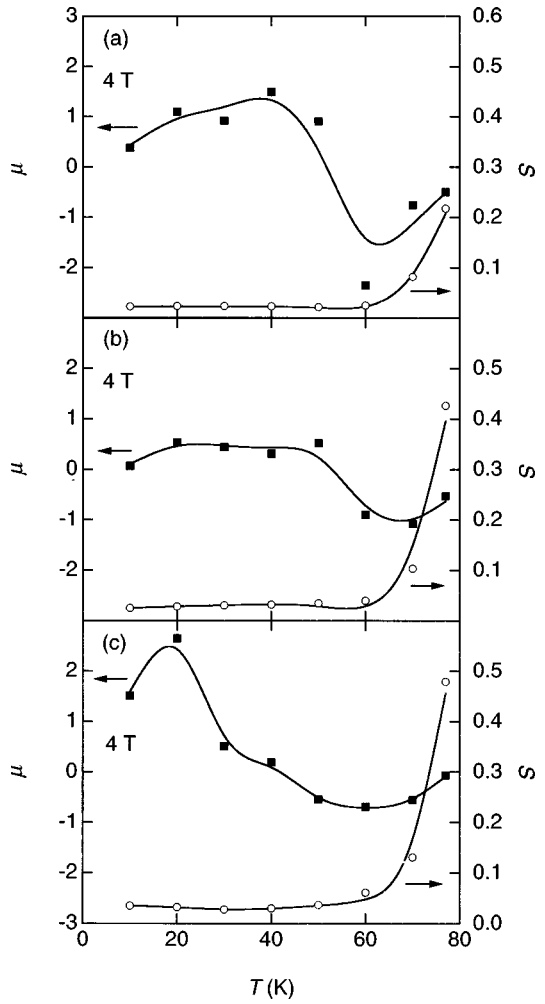

FIG. 5. Temperature dependence of μ and S at 4 T for (a) Nd123SC, (b) OCMG-Nd-Ba-Cu-O, and (c) MPMG-Y-Ba-Cu-O. For all the samples, respective μ and S values are in the range of 0 to 3 and 0.02 to 0.04 at lower temperatures. In contrast, a further increase in temperature leads to a change in the sign of μ values from positive to negative accompanied by an abrupt increase in S. These two regimes correspond to a collective creep regime at lower temperatures and a Kim-Anderson creep regime at higher temperatures.

sistent with the S-T behavior in our previous papers[43,44] and also supports the idea of the collective creep expressed in Eq. (10), as pointed out by Malozemoff and Fisher.[45] Further increase in temperature leads to an abrupt increase in S, which can be explained in terms of the Kim-Anderson creep. These results, therefore, suggest the transition from a collective creep regime to a Kim-Anderson creep regime with increasing temperatures, which agrees well with the results for a Y123 single crystal and a melt-processed Y-Ba-Cu-O bulk reported by Küpfer *et al.*[46]

We then determined fitting parameters in Eq. (9) for these two regimes. Following the approach by Thompson *et al.*[42] we assume that J_{c0} and U_0 vary with temperature as

$$J_{c0}(T)=J_{c0}(0)[1-(T/T_c)^2]^{3/2}, \tag{11}$$

and

$$U_0(T)=U_0(0)[1-(T/T_c)^2]^{3/2}. \tag{12}$$

Equation (11) is deduced from the relation $J_{c0}\approx H_c/\lambda$, where H_c and λ are the thermodynamical critical field ($\propto[1-(T/T_c)^2]$) and the penetration depth ($\propto[1-(T/T_c)^2]^{-1/2}$), respectively. In addition, for simplicity, we use the same exponent $\frac{3}{2}$ to describe T dependence of the potential U_0. First, $U_0(0)$ and $\mu\ln(t/t_{\rm eff})$ were calculated with the least-square method for Eq. (10). These values were substituted into Eq. (9) and then the least-square method was repeated to determine $J_{c0}(0)$, μ, and $\ln(t/t_{\rm eff})$ values. For a high-temperature range, where the Kim-Anderson creep is dominant, Eqs. (6) and (7) were employed in place of Eqs. (9) and (10). Thus, calculated J_c-T curves at 4 T are displayed with the experimental data in Fig. 6. The fitting parameters are listed in Table II. These values are not in contradiction with the previously reported data in Ref. 39. At temperatures approximately below 40 K, the concave curvature is well expressed by the collective creep model, although the true values for $J_{c0}(0)$ and $U_0(0)$ are not empiri-

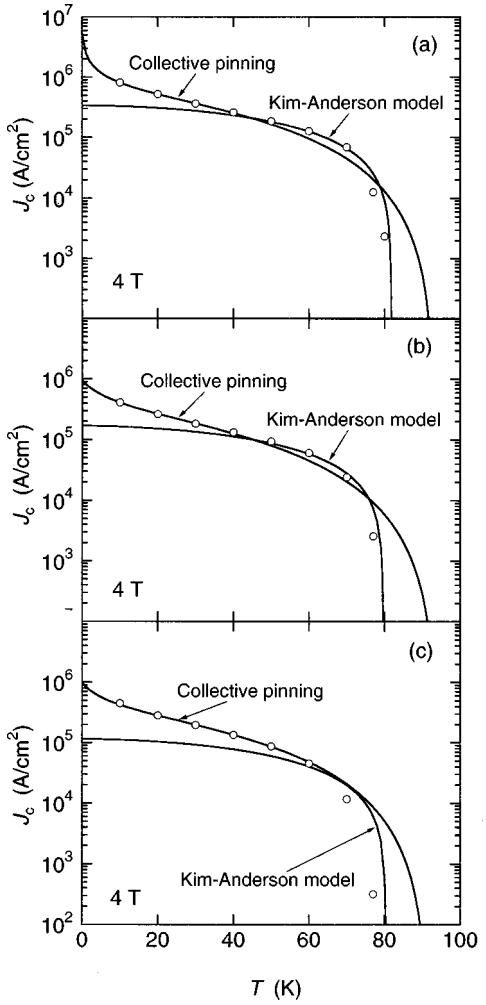

FIG. 6. Fitting of J_c-T behaviors in 4 T with collective creep and Kim-Anderson creep models for (a) Nd123SC, (b) OCMG-Nd-Ba-Cu-O, and (c) MPMG-Y-Ba-Cu-O. The fitting parameters are listed in Table II. Each sample shows a fairly good fitting with two models for all the temperature range.

cally available. In contrast, at temperatures above 50 K, that is a Kim-Anderson regime, it is clear that the sample with higher J_c (or $T_{\rm irr}$) exhibits the larger $J_{c0}(0)$ and $U_0(0)$ values.

In conclusion, the temperature dependence of J_c can totally be explained by taking account of the flux creep combining both the Kim-Anderson and collective creep models. Similar treatment was successfully applied to the understanding of the flux creep in a Y123 single crystal and melt-processed Y123 bulk,[46] therefore, this kind of transition in J_c-T relation might be common to RE123 materials.

C. Field dependence of J_c

In the former section, we showed that the temperature dependence of J_c is well described by taking account of two flux-creep regimes, in which the Kim-Anderson creep is dominant in a high T region, while the collective creep prevails at lower temperatures. Here, it should be born in mind that two parameters U_0 and J_{c0} in Eqs. (5)–(10) are also field dependent, which will be treated in this section.

In a low-field region, since a reduced field b is negligibly small, the field dependence of $J_c \propto B^{\gamma-1}$ is expected from Eq. (4). Figure 7 shows logarithmic replots of J_c vs B at high temperatures above 77 K. It is clear that the relationship $J_c \propto B^{\gamma-1}$ is recognized in a low B region ($B<0.5$ T) for the OCMG-Nd-Ba-Cu-O and MPMG-Y-Ba-Cu-O, where the exponent γ was determined as $\gamma-1\approx-0.7$ to -0.4. On the contrary, the Nd123SC exhibits $\gamma-1\approx-0.1$. For the normal-surface pinning, $\gamma-1=-\frac{1}{2}$ has been deduced theoretically from a simple summation of individual pinning forces.[35] Therefore, it is probable that the high-pinning performance of the OCMG-Nd-Ba-Cu-O and MPMG-Y-Ba-Cu-O in a low B and high T region is closely related to the dispersion of nonsuperconducting particles.

Figure 8 shows logarithmic plots of $J_c/J_{\rm cpk}$ as a function of $B/B_{\rm pk}$ at high temperatures above 60 K for Nd-Ba-Cu-O samples. $B_{\rm pk}$ is the peak field and $J_{\rm cpk}$ is the associated J_c value. In the region of $B/B_{\rm pk}>0.5$, all the curves can be superimposed onto a single curve. Since the J_c-B curves are scaled using $B_{\rm pk}$ as well as $B_{\rm irr}$, it is probable that $B_{\rm pk}$ has temperature dependence similar to $B_{\rm irr}$ and that the pinning mechanism is dominated by a single type of pinning centers. Perkins *et al.*[47] demonstrated that a Tm123 single crystal exhibited this kind of scaling behavior on $J_c/J_{\rm cpk}$ vs $B/B_{\rm pk}$ (or $\Delta M/\Delta M_{\rm pk}$ vs $B/B_{\rm pk}$) plots and tried a semiphenomenological analysis, in which the scaling was successful not only for a wide temperature range but also for varied electric fields E of 10^{-8} to 10^{-7} V m^{-1}. Although M-H curves were not measured with varying E for the present samples, our samples might also exhibit a fishtail behavior even in a higher E. This also suggests that the fishtail effect in RE123 is not due to a change in the flux-creep rate, which has been argued by Schnack *et al.*[48] and by van Dalen *et al.*[49] but to a change in the pinning mechanism, which is consistent with the present results. In a low B region, however, scaling on a

TABLE II. Fitting parameters for $S(T)$ and $J_c(T)$ at 4 T.

Sample	Collective or Kim-Anderson	$J_{c0}(0)$ (MA/cm^2)	$U_0(0)$ (K)	μ	$\ln(t/t_{\rm eff})$
Nd123SC	Collective	4.3	14	1.9	23
	Kim-Anderson	0.34	4.7×10^3	-1 (assumed)	6.4
OCMG-Nd-Ba-Cu-O	Collective	0.95	110	1.6	19
	Kim-Anderson	0.17	4.2×10^3	-1 (assumed)	7.8
MPMG-Y-Ba-Cu-O	Collective	0.96	98	1.7	29
	Kim-Anderson	0.11	3.1×10^3	-1 (assumed)	4.2

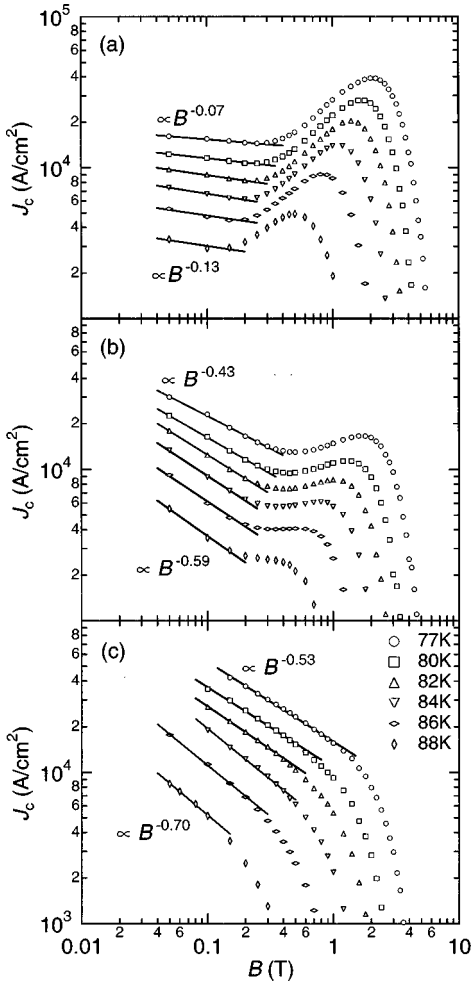

FIG. 7. Logarithmic plots of J_c vs B at temperatures from 77 to 88 K for (a) Nd123SC, (b) OCMG-Nd-Ba-Cu-O, and (c) MPMG-Y-Ba-Cu-O. The relationship $J_c \propto B^{\gamma-1}$ is recognized in a low B region ($B<0.5$ T) for OCMG-Nd-Ba-Cu-O and MPMG-Y-Ba-Cu-O, where $\gamma-1=-0.7$ to -0.4. These values are close to $-\frac{1}{2}$, which is the characteristics for normal surface pinning. On the other hand, the Nd123SC exhibits $\gamma-1\approx-0.1$.

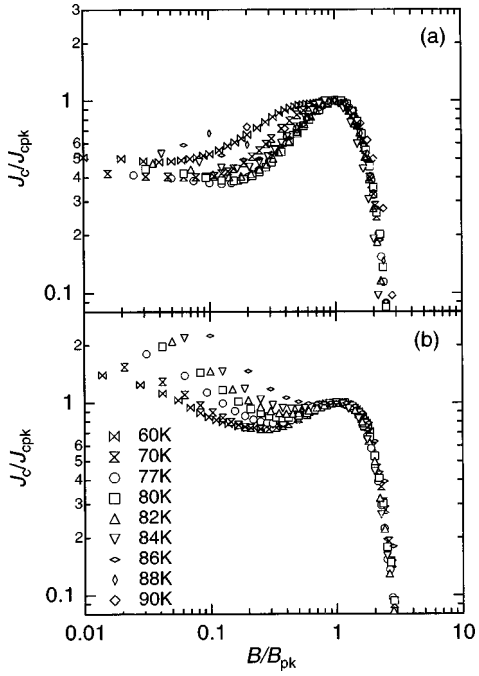

FIG. 8. Logarithmic plots of J_c/J_{cpk} as a function of B/B_{pk} at high temperatures above 60 K for (a) Nd123SC and (b) OCMG-Nd-Ba-Cu-O. In a high B region of $B/B_{pk}>0.5$, all the curves can be superimposed into a single curve. On the other hand, in a low B region, a deviation from the master curve is observed.

single master curve was difficult. This may indicate that dominant pinning centers are different depending on the field range.

Figure 9 shows time decay of M at 70 K for the present samples, in which the M value was normalized by the initial M value. Here, we employed the data at 70 K, since we can neglect the effect of the self field even in 1 T. In a low-field region, concave curves with small slopes are observed, indicating that the collective pinning is dominant in this regime and a creep rate is considerably small. With increasing field, concave curvature is enhanced in the vicinity of the peak field and then it changes to almost a straight line, accompanied by a rapid increase in a creep rate.

Figure 10 displays field dependence of μ and S together with normalized J_c values at 70 K. For Nd123SC, in a field region of $B<B_{pk}$ where J_c increases with B, S is always small and μ is positive, whereas in a region of $B>B_{pk}$, S is large with negative μ. These results also agree with those demonstrated by Küpfer *et al.*[46] Since the J_c-B behaviors are considered to reflect J_{c0} values for $B<B_{pk}$ and relaxation for $B>B_{pk}$, the above-performed analysis based on the $J_c \propto B^{\gamma-1}$ relation will only be adequate in a sufficiently low-field region.

D. Field dependence of F_p

Figure 11 shows logarithmic plots of F_p-B curves at temperatures above 77 K for $H\|c$. F_p increases with increasing B in a low-field regime, where a power-law relation $F_p \propto B^{\gamma}$ is recognized. In an intermediate field range, F_p exhibits a maximum $F_{p\,max}$ at $B=B_{max}$. With further increasing field above B_{max}, F_p decreases and reaches zero at $B=B_{irr}$. In addition, the coordinate at the F_p maximum (B_{max},$F_{p\,max}$) is temperature dependent since both B_{max} and $F_{p\,max}$ decrease with increasing temperature. A comparison of the F_p-B relations among the present samples exhibits two distinct features. One is the presence of a deflection point in the increasing F_p regime for Nd123SC and OCMG-Nd-Ba-Cu-O, which approximately corresponds to the minimum in the J_c-B curves, whereas such a deflection is not observed for MPMG-Y-Ba-Cu-O. The exponent γ values of $F_p \propto B^{\gamma}$ changes from 0.9 to 1.5–1.7 and from 0.4–0.6 to 0.8–1.2 at the deflection point for the Nd123SC and OCMG-Nd-Ba-Cu-O, respectively. Another distinct feature is the exponent γ value of Nd123SC in a low-field region, as observed in the J_c-B behavior in Fig. 7. For Nd123SC, γ is approximately 0.9, while γ values for OCMG-Nd-Ba-Cu-O and MPMG-Y-Ba-Cu-O are in the range of 0.3–0.6. Such a large difference is attributable to the presence of normal second-phase particles in OCMG-Nd-Ba-Cu-O and MPMG-Y-Ba-Cu-O.

In high-temperature superconductors, normalized volume-pinning force f_p ($\equiv F_p/F_{p\,max}$) often scales with B/B_{irr}.

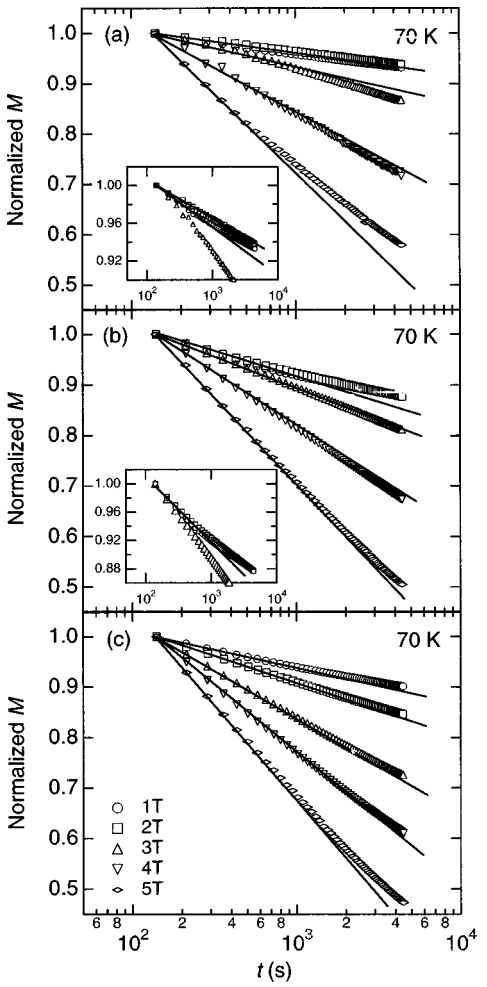

FIG. 9. Time decay of normalized M at 70 K for (a) Nd123SC, (b) OCMG-Nd-Ba-Cu-O, and (c) MPMG-Y-Ba-Cu-O. Here, a temperature of 70 K was selected, since the self-field effect can be neglected even in relatively low fields. At 1 T, concave curves with small slopes are observed. With increasing field, concave curvature is enhanced in the vicinity of the peak field and then becomes almost straight accompanied by a considerable increase in a creep rate.

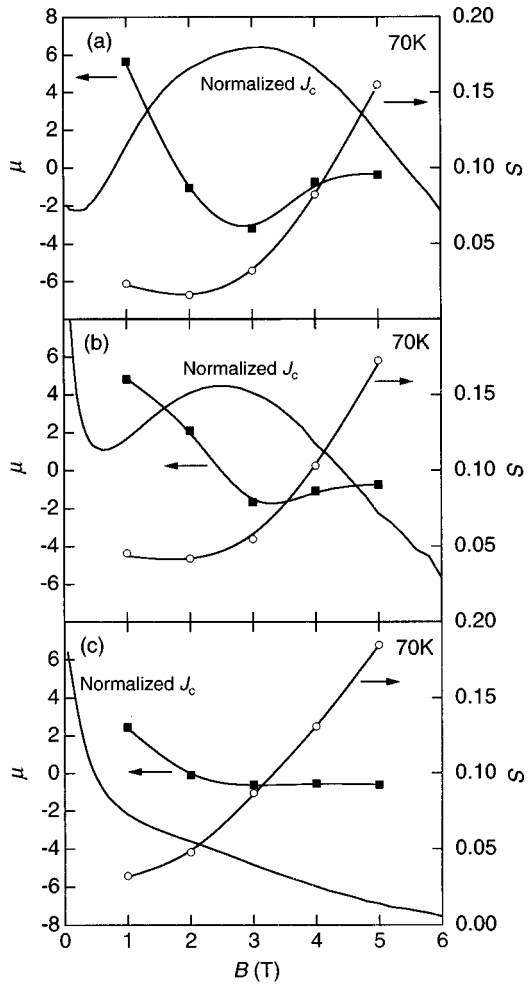

FIG. 10. Field dependence of μ and S together with normalized J_c values at 70 K for (a) Nd123SC, (b) OCMG-Nd-Ba-Cu-O, and (c) MPMG-Y-Ba-Cu-O. For Nd123SC, the increasing J_c regime for $B<B_{\rm pk}$ accompanies small S values and positive μ, whereas the decreasing J_c regime for $B>B_{\rm pk}$ is characterized by large S values and negative μ.

However, it is quite difficult to determine correct $B_{\rm irr}$ values using the dc magnetization measurements. To avoid this inaccuracy, the data were scaled using $B/B_{\rm max}$ ($\equiv b$) instead of $B/B_{\rm irr}$. Figure 12 shows thus obtained plots of f_p vs b at temperatures above 77 K. All the $f_p(b)$ curves for Nd123SC and OCMG-Nd-Ba-Cu-O can be scaled on a single-master curve, suggesting that the dominant pinning mechanism is unchanged in this temperature range. In contrast, the $f_p(b)$ curves at 86 and 88 K exhibit a slight deviation from the master curve in MPMG-Y-Ba-Cu-O, indicating that a different type of pinning centers may become dominant at temperatures close to T_c. In addition, the success in scaling at higher field indicates that $B_{\rm max}$ exhibits an identical temperature dependence with that of $B_{\rm irr}$ and that $B_{\rm max}$ can be used as a scaling field instead of $B_{\rm irr}$.

For Nd123SC and OCMG-Nd-Ba-Cu-O, f_p-b curves are almost symmetrical since f_p merges to zero at $b\approx 2.5$. The symmetrical f_p-b curves are considered as a common feature in Nd samples since it has been observed in other Nd123 single crystals and melt-processed Nd-Ba-Cu-O bulks.[50,51] In contrast, f_p of MPMG-Y-Ba-Cu-O merges to zero at $b\approx 3.5$. For Nd123SC and OCMG-Nd-Ba-Cu-O as indicated by arrows, $b_{\rm pk}$ ($=B_{\rm pk}/B_{\rm max}$), corresponding to the peak field in the J_c-B curves, is located at $b\approx 0.7$. For further evaluation of the field dependence of F_p, the scaling parameters γ and δ in $F_p=F_{\rm p\,max}(B/B_{\rm max})^{\gamma}(1-B/B_{\rm max})^{\delta}$ were calculated from the experimental data. The obtained scaling parameters are listed in Table III. Although Nd123SC and OCMG-Nd-Ba-Cu-O exhibit $\gamma\approx 1-3$ and $\delta\approx 2-5$, MPMG-Y-Ba-Cu-O possesses $\gamma\approx 0.6-0.8$ and $\delta\approx 2-4$. It should also be noted that Nd123SC and OCMG-Nd-Ba-Cu-O show a slight decrease in γ and δ with increasing temperature from 77 to 90 K, which is partly ascribed to the peak broadening in the f_p-b curves.

To interpret a large difference in γ in a low-field region, we first consider the surface pinning by nonsuperconducting particles, whose average diameter is larger than the coherence length ξ. Based on the direct summation of elementary pinning forces, Matsushita[35] has deduced the pinning-force density in a creep-free case (F_{p0}) as

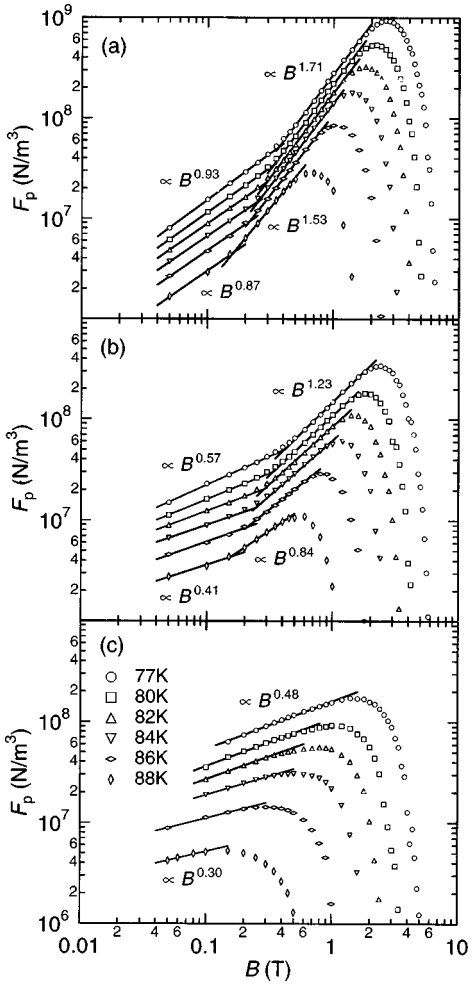

FIG. 11. Logarithmic plots of F_p vs B at high temperatures of 77–88 K for (a) Nd123SC, (b) OCMG-Nd-Ba-Cu-O, and (c) MPMG-Y-Ba-Cu-O. A power law relation $F_p \propto B^{\gamma}$ is recognized in a low-field regime. The exponent γ values changes from 0.9 to 1.5–1.7 and from 0.4–0.6 to 0.8–1.2 at the deflection point for Nd123SC and OCMG-Nd-Ba-Cu-O, respectively. For MPMG-Y-Ba-Cu-O in which the deflection point is absent, γ lies in the range from 0.3 to 0.5.

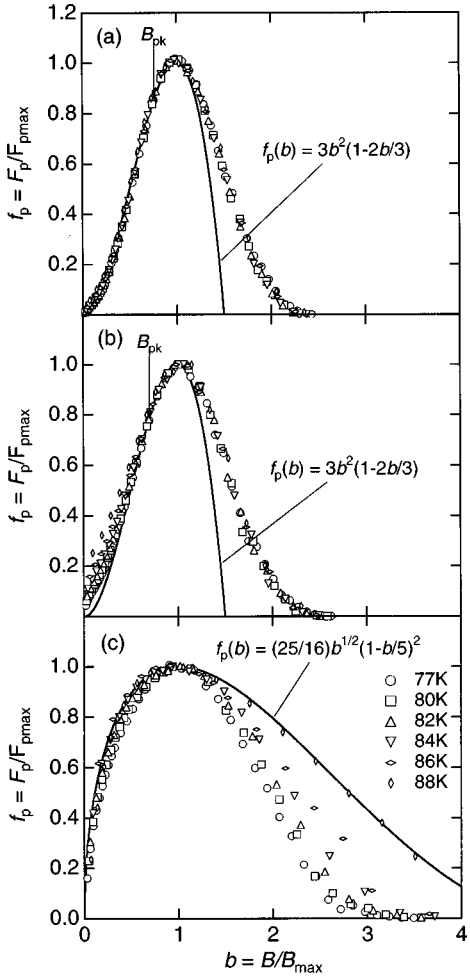

FIG. 12. Plots of f_p vs B/B_{max} $(=b)$ at temperatures of 77–88 K for (a) Nd123SC, (b) OCMG-Nd-Ba-Cu-O, and (c) MPMG-Y-Ba-Cu-O. For Nd123SC and OCMG-Nd-Ba-Cu-O, as indicated by arrows, b_{pk} $(=B_{pk}/B_{max})$, corresponding to the peak field in the J_c-B curves, is located at around $b \approx 0.7$. The scaling parameters γ and δ in $F_p = F_{p\,max}(B/B_{max})^{\gamma}(1-B/B_{max})^{\delta}$ are listed in Table III.

$$F_{p0} = \pi B_c^2 N D^2 \xi/(4\mu_0 a_f)\ \ (1-B/B_{c2})^2, \qquad (13)$$

where B_c is the thermodynamic critical field, N the density of nonsuperconducting particles, D their mean size, a_f the flux-line lattice spacing, and ξ the coherence length along the direction of the flowing current. Thus, obtained expression in Eq. (13) is a special case of the general expression Eq. (3), where $m=3/2$, $\gamma=1/2$, and $\delta=2$, since $B_c(T) \propto B_{c2}(T)$, $\xi \propto B_{c2}^{-1/2}$, $B_{c2} \propto 1-(T/T_c)^2$, and $a_f \propto B^{-1/2}$. Experimentally obtained γ values for OCMG-Nd-Ba-Cu-O and MPMG-Y-Ba-Cu-O are nearly equal to $\gamma=\frac{1}{2}$, supporting the fact that the dominant pinning for these systems is core pinning by 123/211 (or 422) interfaces.

In contrast, Nd123SC exhibits the higher γ values of approximately 0.9, which clearly shows that the dominant pinning centers are different and will be microscopic features such as cation or oxygen defects, and twin planes. In a low-field regime, if the spacing of pinning centers is smaller than a_f, every vortex can interact with a pinning center. In this case, F_{p0} is proportional to $1/a_f^2$, resulting in $F_{p0} \propto B$ with $\gamma=1$. Dew-Hughes[52] has also deduced $F_{p0}(B)$ for the normal point pinning, which corresponds to the case of $\gamma=1$ and has the form:

$$F_{p0} = V_f B_{c2}^2 (B/B_{c2})(1-B/B_{c2})^2/(256\mu_0 a \kappa^2), \qquad (14)$$

where V_f is the volume fraction of the superconductor, a the size of the pinning centers, and κ the Ginzburg-Landau parameter. Wen and Zhao[53] have also obtained a similar expression, in which F_{p0} is proportional to $B/B_{irr}(1-B/B_{irr})^2$, and reaches a maximum at $B/B_{irr}=0.33$, on the assumption that most pinning centers are small-sized normal cores. Thus, the γ value of ≈ 0.9 suggests that normal point-pinning centers are mainly active in Nd123SC at low fields.

Next, we treat f_p-b behavior in an intermediate-field region. According to Klein *et al.*,[12] based on $\Delta\kappa$ pinning,[52] $f_p(b)$ has the form:

$$f_p(b) = 3b^2(1-2b/3), \qquad (15)$$

where $b=B/B_{max}$. In the $\Delta\kappa$ pinning, since a difference in the condensation energy between high and low κ regions leads to pinning, F_{p0} has the form:

TABLE III. Scaling parameters γ and δ in $F_p = F_{p\,max}(B/B_{max})^{\gamma}(1-B/B_{max})^{\delta}$.

Temperature (K)	Nd123SC		OCMG-Nd-Ba-Cu-O		MPMG-Y-Ba-Cu-O	
	γ	δ	γ	δ	γ	δ
77	2.83±0.08	4.93±0.38	2.38±0.10	3.98±0.46	0.71±0.05	2.30±0.40
80	2.83±0.07	4.62±0.31	2.37±0.12	3.76±0.51	0.82±0.05	2.59±0.45
82	2.90±0.06	4.75±0.28	2.18±0.14	3.30±0.54	0.76±0.05	2.33±0.36
84	2.75±0.08	4.27±0.34	2.15±0.12	3.22±0.47	0.67±0.04	2.12±0.27
86	2.74±0.09	4.55±0.44	2.02±0.13	2.96±0.50	0.62±0.05	2.43±0.48
88	2.51±0.07	4.08±0.36	1.75±0.16	2.28±0.48	0.68±0.04	3.97±0.91
90	2.27±0.01	3.86±0.50	1.34±0.14	2.03±0.41		

$$F_{p0} = V_f B_{c2}^2 (B/B_{c2})^2 (1-B/B_{c2}) \Delta\kappa/(64\mu_0 a \kappa^3). \quad (16)$$

This field dependence clearly shows that F_{p0} increases with b in the form of $F_{p0} \propto b^2$ in an intermediate-field regime. Hiergeist and Hergt[54] deduced the value $\gamma = \frac{7}{4}$ on the basis of collective pinning by random-point pins. However, as pointed out by Klein *et al.*,[12] in this interpretation the scaling holds only to B_{max}, and, therefore, deviation from the scaled master curve may take place at higher fields, which in fact has already been observed in Y123 single crystals with the peak effect as reported by Hyun *et al.*[55] It is probable that the flux creep is responsible for such a deviation, since the experimental data are not normalized by B_{c2}. It is also probable that, as pointed out by Perkins *et al.*[47] and Klein *et al.*,[12] J_c (and automatically F_p) is dependent on the electrical field E and, therefore, the scaling of J_c-B curves is also E dependent.

It is interesting to note that unlike Y123 single crystals the f_p-b curves of the Nd123SC and OCMG-Nd-Ba-Cu-O samples can be scaled on the same master curve in a higher-field region ($B > B_{max}$). Therefore, it is probable that these two samples have an identical pinning mechanism originating from the Nd123 matrix itself for this field range, although in a low-field region normal-surface pinning is dominant in OCMG-Nd-Ba-Cu-O.

On the other hand, f_p-b data for MPMG-Y-Ba-Cu-O varies as

$$f_p(b) = (25/16) b^{1/2} (1-b/5)^2, \quad (17)$$

where $b = B/B_{max}$. This expression is identical to the previously suggested equation $f_p \propto (B/B_{irr})^{1/2}(1-B/B_{irr})^2$,[35] and also has a form similar to that proposed by Kramer,[56] in which the flux motion is dominated by synchronous shear of the FLL at lower fields and by plastic deformation of FLL at higher fields, although B is normalized by B_{c2} instead of B_{irr}.

E. Comparison of flux-pinning mechanism in RE123 (RE=Y,Nd) systems

It is evident that a single expression of either Eqs. (13), (14), or (16) will not cover the field and temperature dependences of J_c and F_p in the whole (B,T) range, however, the pinning performance of the present samples can be characterized by several (B,T) regions.

In a low-field region, Nd123SC exhibits the relation $F_p \propto B$, indicating that the normal point pinning is dominant, while OCMG-Nd-Ba-Cu-O and MPMG-Y-Ba-Cu-O exhibit the relation $F_p \propto B^{1/2}$, indicating that normal surface pinning is dominant, which is attributable to the presence of relatively large normal inclusions of Nd422 or Y211 as proposed by Murakami *et al.*[57] For Nd123SC, microscopic features such as cation or oxygen defects, and twin planes are believed to be the sources of normal point pinning. In contrast, the pinning by twin planes at low fields in OCMG-Nd-Ba-Cu-O and MPMG-Y-Ba-Cu-O will be negligibly small due to the presence of more effective pinning centers like Nd422 and Y211 inclusions.

In a high-temperature and intermediate-field region, $\Delta\kappa$ point pinning ($F_p \propto B^2$) is dominant for Nd123SC and OCMG-Nd-Ba-Cu-O, while normal surface pinning ($F_p \propto B^{1/2}$) remains dominant for MPMG-Y-Ba-Cu-O. It has been pointed out that oxygen-deficient regions with depressed T_c cause the fishtail effect in M-H loops.[11] In general, the presence of a small region that has condensation energy slightly smaller than that of the matrix is responsible for field-induced pinning and thus the fishtail effect. Hyun *et al.*[55] proposed that a slight Mg contamination on the Y site was responsible for the fishtail effect based on the fact that the full oxygenation did not eliminate the fishtail peak in the Y123 single crystals grown in a MgO crucible. In addition to the fact that prolonged oxygenation did not eliminate the fishtail peak,[1] a good fitting with the $\Delta\kappa$ point-pinning model in the intermediate-field region supports our idea that field-induced pinning by Nd-Ba substituted regions causes the fishtail effect in Nd-Ba-Cu-O. Another possible origin of the fishtail effect is Y substitution on Nd sites from the YSZ crucible during the crystal growth. However, electron-probe microanalyses revealed that Y contamination is very small in the present Nd123 crystal so that the effect of Y contamination can be discarded as the source of the fishtail effect.

In a low-temperature region, the temperature dependence of J_c (or F_p) could well be explained in terms of the collective flux-creep model, although it was difficult to study the scaling behavior of f_p-b curves in a full-scale range, since the irreversibility fields were much higher than the maximum field available in a SQUID magnetometer. It is interesting to note that at low temperatures the temperature dependences of thermodynamic parameters such as the critical field and the coherence length seem to prevail the J_c-T behavior rather than the pinning performance.

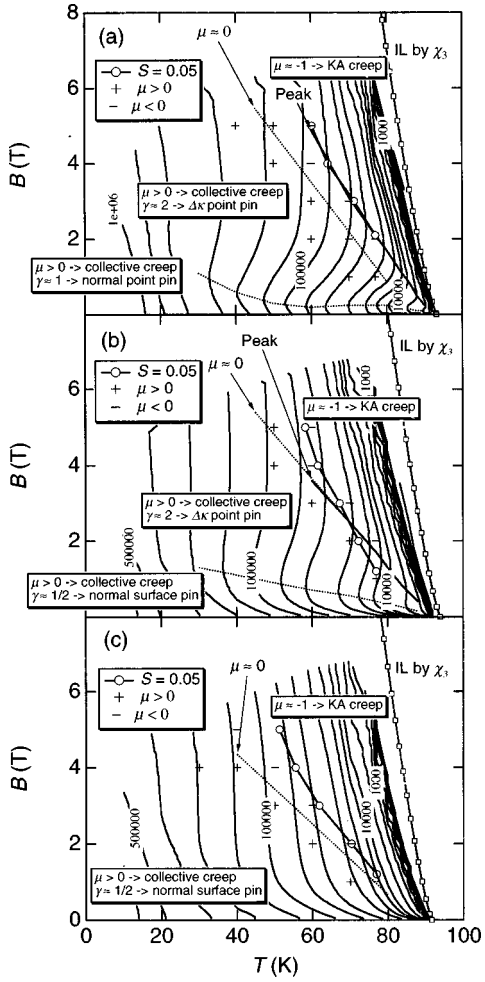

FIG. 13. B-T phase diagrams with a contour map of constant J_c curves and the boundary lines of $\mu \approx 0$ and $S = 0.05$ for (a) Nd123SC, (b) OCMG-Nd-Ba-Cu-O, and (c) MPMG-Y-Ba-Cu-O. The lines for $\mu \approx 0$ were determined as a boundary at which the sign of μ value changes from positive to negative. The lines for $S = 0.05$ correspond to a threshold above which a rapid increase in S is observed.

Figure 13 shows B-T phase diagrams together with the contour of constant J_c curves. As a reference, the B_{irr} values determined from the onset of the third-harmonic response χ_3 to ac field, which were reported for the present samples in our previous paper,[58] are plotted together. In addition, the boundary lines corresponding to $\mu \approx 0$ and $S = 0.05$ are drawn in the figure. The lines for $\mu \approx 0$ correspond to the crossover point of μ values from positive to negative and thus a transition from collective to Kim-Anderson (KA) creep regimes. The lines for $S = 0.05$ correspond to the point at which a rapid increase in S is observed. For Nd-Ba-Cu-O samples, the lines for $S = 0.05$ approximately lie on the peak position. For MPMG-Y-Ba-Cu-O without the fishtail behavior, both the lines for $\mu \approx 0$ and $S = 0.05$ are located at relatively lower fields and temperatures. It is also interesting to note that the lines for $S = 0.05$ and $\mu \approx 0$ were closely positioned to each other for all the samples, indicating that the transition from collective to KA creep is accompanied by an abrupt increase in S.

Consequently, the pinning characteristics with increasing fields at constant temperatures are summarized as follows: normal-point pinning–$\Delta\kappa$ point pinning–KA creep for Nd123SC, normal-surface pinning-KA creep for MPMG-Y-Ba-Cu-O, and normal-surface pinning–$\Delta\kappa$ point pinning–KA creep for OCMG-Nd-Ba-Cu-O. The transition from single-vortex to collective pinning has been proposed in Ref. 10, in which the H-T phase diagram is subsectioned into two regimes: a single-vortex pinning regime below the temperature T_{sv} and a collective-pinning regime above T_{sv}. In the present paper, however, the presence of the transition from single-vortex to collective pinning was not so evident, since the values of J_c, S, and μ in the low-field and temperature regime could not be defined owing to the self-field effect or the experimental limits in the M-H measurements.

For thorough understanding of the pinning performance in the RE123 system, anisotropic pinning behavior by the twin planes should be taken into consideration. For example, in a recent study on J_c-B properties of Nd123 single crystals and melt-textured samples with high-irreversibility fields,[59] a strong angular dependence of the peak effect suggests the significance of pinning by twin planes. Also in our Nd123 single crystals, some other samples exhibit an anomalous peak appearance in an intermediate temperature range,[17] which is sensitive to the angle between the flux and the c axis.

IV. CONCLUSIONS

We have performed a comparative study of flux-pinning behaviors among the Nd123SC, OCMG-Nd-Ba-Cu-O and MPMG-Y-Ba-Cu-O samples. Based on temperature dependence of J_c, μ, and S, an exponential-like J_c behavior accompanied by positive μ and temperature-independent S in a low T region for all the samples was described using the collective flux-creep model. In a high T region, a decrease in J_c, negative μ and increase in S with T could be explained in terms of the Kim-Anderson creep model. As for the field dependence, the exponent γ in a power relation of $J_c \propto B^{\gamma-1}$ or $F_p \propto B^{\gamma}$ in a low-field regime, where positive μ and smaller S were observed, changed from 0.9 to 1.5–1.7 and from 0.4–0.6 to 0.8–1.2 at the deflection point for Nd123SC and OCMG-Nd-Ba-Cu-O, respectively. The γ value for MPMG-Y-Ba-Cu-O ranged from 0.3 to 0.6 without the deflection point. These results allow us to assign the dominant pinning mechanism to several (B,T) regimes. First, the peak behavior, which is observed in a high B and high T region for Nd123SC and OCMG-Nd-Ba-Cu-O, is ascribed to the $\Delta\kappa$ point pinning. Second, in a low B and high T region for OCMG-Nd-Ba-Cu-O and MPMG-Y-Ba-Cu-O, in which a monotonous decrease in J_c with increasing B is observed, the normal surface pinning by the Nd422 or Y211 inclusions is dominant. In contrast, for Nd123SC, the normal point pinning seems dominant in a low B and high T region, where J_c is almost B independent. In a low T region, although the field dependence of J_c could not be measured in a full range due to the experimental limits in the M-H measurements, the temperature dependence of J_c could be described in terms of the collective flux creep.

ACKNOWLEDGMENTS

The authors would like to thank H. Fujimoto in Railway Technical Research Institute, M. R. Koblischka, N. Chikumoto, and T. Mochida in Superconductivity Research Laboratory (SRL) for fruitful discussions, K. Sawada and N. Hayashi in SRL for sample preparation, and K. Waki in SRL for his help in the magnetization measurements. This paper was partially supported by New Energy and Industrial Technology Development Organization (NEDO) for the R&D of Industrial Science and Technology Frontier Program.

[1] See, e.g., S. I. Yoo and M. Murakami, *Recent Research Developments in Cryogenics* (Research Signpost Publisher Inc., Trivandrum, India, 1996), p. 29; M. Murakami, N. Sakai, T. Higuchi, and S. I. Yoo, Supercond. Sci. Technol. **9**, 1015 (1996).

[2] N. Sakai, S. Goshima, M. Kawaguchi, S. I. Yoo, and M. Murakami, Mater. Sci. Eng. B **53**, 109 (1998).

[3] T. Saitoh, K. Segawa, K. Kamada, N. Sakai, T. Segawa, S. I. Yoo, and M. Murakami, Physica C **288**, 141 (1997).

[4] M. Muralidhar, H. S. Chauhan, T. Saitoh, K. Kamada, K. Segawa, and M. Murakami, Supercond. Sci. Technol. **10**, 663 (1997).

[5] T. Egi, J. G. Wen, K. Kuroda, H. Mori, H. Unoki, and N. Koshizuka, Physica C **270**, 223 (1996); T. Egi, J. G. Wen, Wu Ting, T. Higuchi, S. I. Yoo, K. Kuroda, H. Unoki, M. Murakami, and N. Koshizuka, *Advances in Superconductivity VIII* (Springer-Verlag, Tokyo, 1996), p. 465.

[6] T. Higuchi, S. I. Yoo, K. Sawada, N. Sakai, and M. Murakami, Physica C **263**, 396 (1996).

[7] S. I. Yoo and R. W. McCallum, Physica C **210**, 147 (1993).

[8] Wu Ting, T. Egi, K. Kuroda, N. Koshizuka, and S. Tanaka, Appl. Phys. Lett. **70**, 770 (1997).

[9] N. Chikumoto, J. Yoshioka, M. Otsuka, N. Hayashi, and M. Murakami, Physica C **281**, 253 (1997).

[10] L. Krusin-Elbaum, L. Civale, V. M. Vinokur, and F. Holtzberg, Phys. Rev. Lett. **69**, 2280 (1992).

[11] M. Daeumling, J. M. Seuntjens, and D. C. Larbalestier, Nature (London) **346**, 332 (1990).

[12] L. Klein, E. R. Yacoby, Y. Yeshurun, A. Erb, G. Müller-Vogt, V. Breit, and H. Wühl, Phys. Rev. B **49**, 4403 (1994).

[13] H. H. Wen, X. S. Rong, B. Yin, G. C. Che, and Z. X. Zhao, Physica C **242**, 365 (1995).

[14] L. Civale, M. W. McElfresh, A. D. Marwick, F. Holtzberg, and C. Feild, Phys. Rev. B **43**, 13 732 (1991).

[15] K. Kishio, J. Shimoyama, Y. Kotaka, and K. Yamafuji, in *Proceedings of the 7th International Workshop on Critical Currents in Superconductors* (World Scientific, Singapore, 1994), p. 339.

[16] A. Erb, E. Walker, J.-Y. Genoud, and R. Flükiger, Physica C **282–287**, 89 (1997).

[17] M. R. Koblischka, A. J. J. van Dalen, T. Higuchi, K. Sawada, S. I. Yoo, and M. Murakami, Phys. Rev. B **54**, R6893 (1996).

[18] H. Kojo, S. I. Yoo, N. Sakai, and M. Murakami, Superlattices Microstruct. **21**, 37 (1997).

[19] S. Jin, T. H. Tiefel, R. C. Sherwood, R. B. van Dover, M. E. Davis, G. W. Kammlott, and R. A. Fastnacht, Phys. Rev. B **37**, 7850 (1988); K. Salama, V. Selvamanickam, L. Gao, and K. Sun, Appl. Phys. Lett. **54**, 2352 (1989).

[20] M. Murakami, M. Morita, and N. Koyama, Jpn. J. Appl. Phys., Part 2 **28**, L1125 (1989).

[21] H. Fujimoto, M. Murakami, S. Gotoh, N. Koshizuka, T. Oyama, Y. Shiohara, and S. Tanaka, *Advances in Superconductivity II* (Springer-Verlag, Tokyo, 1990), p. 285.

[22] P. W. Anderson, Phys. Rev. B **9**, 309 (1962).

[23] M. P. A. Fisher, Phys. Rev. Lett. **62**, 1415 (1989); D. S. Fisher, M. P. A. Fisher, and D. A. Huse, Phys. Rev. B **43**, 130 (1991).

[24] M. V. Feigel'man, V. B. Geshkenbein, A. I. Larkin, and V. M. Vinokur, Phys. Rev. Lett. **63**, 2303 (1989); M. V. Feigel'man and V. M. Vinokur, Phys. Rev. B **41**, 8986 (1990); M. V. Feigel'man, V. B. Geshkenbein, and V. M. Vinokur, *ibid.* **43**, 6263 (1991).

[25] A. I. Larkin and Yu. N. Ovchinikov, J. Low Temp. Phys. **34**, 409 (1979).

[26] G. Blatter, M. V. Feigel'man, V. B. Geshkenbein, A. I. Larkin, and V. M. Vinokur, Rev. Mod. Phys. **66**, 1125 (1994).

[27] S. Sawada, S. I. Yoo, N. Sakai, T. Higuchi, and M. Murakami, *Fourth European Ceramics VI* (Gruppo Editoriale Faenza Editrice S.p.A., Italy, 1995), p. 293.

[28] N. Chikumoto, S. Ozawa, S. I. Yoo, N. Hayashi, and M. Murakami, Physica C **278**, 187 (1997).

[29] K. Kishio, J. Shimoyama, T. Hasegawa, K. Kitazawa, and K. Fueki, Jpn. J. Appl. Phys., Part 2 **26**, L1228 (1987).

[30] K. Takita, H. Katoh, H. Akinaga, M. Nishino, T. Ishigaki, and H. Asano, Jpn. J. Appl. Phys., Part 2 **27**, L57 (1988).

[31] L. Civale, L. Krusin-Elbaum, J. R. Thompson, and F. Holtzberg, Phys. Rev. B **50**, 7188 (1994).

[32] E. M. Gyorgy, R. B. van Dover, K. A. Jackson, L. F. Schneemeyer, and J. V. Waszczak, Appl. Phys. Lett. **55**, 283 (1989).

[33] L. W. Conner and A. P. Malozemoff, Phys. Rev. B **43**, 402 (1991).

[34] A. D. Caplin, L. F. Cohen, G. K. Perkins, and A. A. Zhukov, Supercond. Sci. Technol. **7**, 412 (1994).

[35] T. Matsushita, Physica C **205**, 289 (1993); N. Ihara and T. Matsushita, *ibid.* **257**, 223 (1996); M. Kiuchi, E. S. Otabe, T. Matsushita, T. Kato, T. Hikata, and K. Sato, *ibid.* **260**, 177 (1996).

[36] T. Higuchi, S. I. Yoo, K. Waki, H. Fujimoto, and M. Murakami, Physica C **282–287**, 2137 (1997).

[37] P. Manuel, C. Aguillon, and S. Senoussi, Physica C **177**, 281 (1991).

[38] L. A. Dorosinskii, V. I. Nikitenko, A. A. Polyanskii, and V. K. Vlasko-Vlasov, Physica C **219**, 81 (1994).

[39] J. R. Thompson, Yang Ren Sun, L. Civale, A. P. Malozemoff, M. W. McElfresh, A. D. Marwick, and F. Holtzberg, Phys. Rev. B **47**, 14 440 (1993).

[40] E. Zeldov, N. M. Amer, G. Koren, A. Gupta, M. W. McElfresh, and R. J. Gambino, Appl. Phys. Lett. **56**, 680 (1990).

[41] M. P. Maley, J. O. Willis, H. Lessure, and M. E. McHenry, Phys. Rev. B **42**, 2639 (1990).

[42] J. R. Thompson, Yang Ren Sun, and F. Holtzberg, Phys. Rev. B **44**, 458 (1991); J. R. Thompson, Yang Ren Sun, D. K. Christen, L. Civale, A. D. Marwick, and F. Holtzberg, *ibid.* **49**, 13 287 (1994); Yang Ren Sun, J. R. Thompson, Y. J. Chen, D. K. Christen, and A. Goyal, *ibid.* **47**, 14 481 (1993).

[43] A. J. J. van Dalen, M. R. Koblischka, H. Kojo, K. Sawada, T.

Higuchi, and M. Murakami, Supercond. Sci. Technol. **9**, 659 (1996).
[44] T. Mochida and M. Murakami, Physica C **290**, 311 (1997).
[45] A. P. Malozemoff and M. P. A. Fisher, Phys. Rev. B **42**, 6784 (1990).
[46] H. Küpfer, S. N. Gordeev, W. Jahn, R. Kresse, R. Meier-Hirmer, T. Wolf, A. A. Zhukov, K. Salama, and D. Lee, Phys. Rev. B **50**, 7016 (1994).
[47] G. K. Perkins, L. F. Cohen, A. A. Zhukov, and A. D. Caplin, Phys. Rev. B **51**, 8513 (1995).
[48] H. G. Schnack, R. Griessen, J. G. Lensink, and H. H. Wen, Phys. Rev. B **48**, 13 178 (1993).
[49] A. J. J. van Dalen, M. R. Koblischka, R. Griessen, M. Jirsa, and G. Ravi Kumar, Physica C **250**, 265 (1995).
[50] M. R. Koblischka, Physica C **282-287**, 2193 (1997).
[51] M. R. Koblischka, A. J. J. van Dalen, T. Higuchi, S. I. Yoo, and M. Murakami, Phys. Rev. B **58**, 2863 (1998).
[52] D. Dew-Hughes, Philos. Mag. **30**, 293 (1974).
[53] H. H. Wen and Z. X. Zhao, Appl. Phys. Lett. **68**, 856 (1996).
[54] R. Hiergeist and R. Hergt, Phys. Rev. B **55**, 3258 (1997).
[55] O. B. Hyun, M. Yoshida, T. Kitamura, and I. Hirabayashi, Physica C **258**, 365 (1996).
[56] E. J. Kramer, J. Appl. Phys. **44**, 1360 (1973).
[57] M. Murakami, S. Gotoh, H. Fujimoto, K. Yamaguchi, N. Koshizuka, and S. Tanaka, Supercond. Sci. Technol. **4**, S43 (1991).
[58] K. Waki, T. Higuchi, S. I. Yoo, M. Watahiki, N. Hayashi, N. Sakai, N. Chikumoto, and M. Murakami, Cryogenics **37**, 643 (1997).
[59] Th. Wolf, A-C. Bornarel, H. Küpfer, R. Meier-Hirmer, and B. Obst, Phys. Rev. B **56**, 6308 (1997).